Author(s): Leino, Teppo O.; Turku, Ainoleena; Urvas, Lauri; Adhikari, Karuna; Oksanen, Jouni; Steynen, Yana; Yli-Kauhaluoma, Jari; Xhaard, Henri; Kukkonen, Jyrki P.; Wallén, Erik A. A.

Title: Azulene as a biphenyl mimetic in orexin/hypocretin receptor agonists

Year: 2023

Version: Published version

Leino, T. O., Turku, A., Urvas, L., Adhikari, K., Oksanen, J., Steynen, Y., Yli-Kauhaluoma, J., Xhaard, H., Kukkonen, J. P., & Wallén, E. A.A. (2023). Azulene as a biphenyl mimetic in orexin/hypocretin receptor agonists. Bioorganic and Medicinal Chemistry, 88-89, Article 117325. https://doi.org/10.1016/j.bmc.2023.117325

Bioorg. Med. Chem. 88–89 (2023) 117325

Contents lists available at ScienceDirect

Bioorganic & Medicinal Chemistry

journal homepage: www.elsevier.com/locate/bmc

Azulene as a biphenyl mimetic in orexin/hypocretin receptor agonists

Teppo O. Leino [a,b,*,1], Ainoleena Turku [a,c,1,2], Lauri Urvas [a,d,3], Karuna Adhikari [a], Jouni Oksanen [a], Yana Steynen [a], Jari Yli-Kauhaluoma [a], Henri Xhaard [a], Jyrki P. Kukkonen [c,d], Erik A.A. Wallén [a]

[a] Drug Research Program, Division of Pharmaceutical Chemistry and Technology, Faculty of Pharmacy, University of Helsinki, P.O. Box 56, FI-00014 University of Helsinki, Finland
[b] Department of Chemistry and NanoScience Center, University of Jyväskylä, P.O. Box 35, FI-40014 University of Jyväskylä, Finland
[c] Department of Veterinary Biosciences, Faculty of Veterinary Medicine, University of Helsinki, P.O. Box 66, FI-00014 University of Helsinki, Finland
[d] Department of Pharmacology, Faculty of Medicine, University of Helsinki, P.O. Box 63, FI-00014 University of Helsinki, Finland

ARTICLE INFO

Keywords:
Agonist
Azulene
Medicinal chemistry
Orexin receptor
Sulfonamides

ABSTRACT

Azulene is a rare ring structure in drugs, and we investigated whether it could be used as a biphenyl mimetic in known orexin receptor agonist **Nag 26**, which is binding to both orexin receptors OX_1 and OX_2 with preference towards OX_2. The most potent azulene-based compound was identified as an OX_1 orexin receptor agonist (pEC_{50} = 5.79 ± 0.07, maximum response = 81 ± 8% (s.e.m. of five independent experiments) of the maximum response to orexin-A in Ca^{2+} elevation assay). However, the azulene ring and the biphenyl scaffold are not identical in their spatial shape and electron distribution, and their derivatives may adopt different binding modes in the binding site.

1. Introduction

The orexin/hypocretin system, which consists of two orexin receptors (OX_1 and OX_2) and their endogenous peptide-ligands orexin-A and orexin-B,[1–2] plays a part in many physiological functions, such as sleep–wake regulation, analgesia, stress response, motivational behaviour and addiction, and feeding and metabolic regulation.[3–7] Its central role in sleep-wake regulation has raised interest in orexin receptor antagonists as a novel class of hypnotics, now already realized as two compounds in the clinical use.[8–9] On the other hand, a study in a mouse model of narcolepsy has demonstrated that orexin receptor agonists may prove advantageous as a treatment for narcolepsy.[10] Furthermore, OX_1 activation is linked to anti-proliferation in some colorectal cancer cell lines suggesting that OX_1 agonists could be beneficial for cancer treatment.[11–15] Unlike antagonists, agonists have gained attention in drug discovery only recently, and a few series of potent small molecular orexin receptor agonists have been reported in the literature so far.[16–21] The first series was published in 2015 with **Nag 26** (**1**) as the most potent compound in it (Figure 1).[16,22]

Nag 26, like several other potent orexin receptor agonists, has a biphenyl scaffold.[16,19–21] As a consequence of replacing the amide-substituted phenyl moiety of the biphenyl in **Nag 26** with heteroaromatic five- or six-membered ring, or alkyl group, the activity towards both receptor subtypes has decreased or completely abrogated.[19] The first reported orexin receptor small molecule agonists, including **Nag 26**, have been OX_2-selective,[16–18] and not until 2021 a potent dual orexin receptor agonist, **RTOXA-43** (**2**), a derivative of **Nag 26**, was discovered.[19] **RTOXA-43** was obtained by modifying the dimethylcarbamoyl group of **Nag 26** (Figure 1). Restriction of the bond rotation in **Nag 26** using naphthalene in place of *N*-phenylethylenediamine moiety has produced a potent and OX_2-selective agonist **3**.[20] In addition, replacement of the naphthalene moiety in **3** with tetralin has led to the discovery of compound **4**, which is not only a potent OX_2 but also potent OX_1 agonist.[21] The first potent OX_1-selective agonist **5**, based on compound **4** with modifications on the biphenyl part of the molecule, has been reported recently.[23]

Azulene is a bicyclic aromatic hydrocarbon, which has not been intensively employed ring structure in drug molecules. We have

* Corresponding author at: Department of Chemistry and NanoScience Center, University of Jyväskylä, P.O. Box 35, FI-40014 University of Jyväskylä, Finland.
E-mail address: teppo.o.leino@jyu.fi (T.O. Leino).
[1] These authors contributed equally to this work.
[2] Present Address: Orion Pharma R&D, Espoo, Finland.
[3] Present Address: Laboratoire d'Innovation Thérapeutique, UMR 7200 CNRS, Université de Strasbourg, Illkirch, France.

https://doi.org/10.1016/j.bmc.2023.117325
Received 2 February 2023; Received in revised form 26 April 2023; Accepted 5 May 2023
Available online 9 May 2023

previously studied the applicability of azulene structure in medicinal chemistry, and shown that azulene scaffold does not have any general liabilities to hinder its use in drug discovery.[24] Inspired by this fact, we have studied azulene-based compounds as orexin receptor ligands.[25–26] These compounds indicate a benzoyl group in the 1-position and an ester group in the 6-position of the azulene scaffold as the most important functionalities for the observed weak orexin receptor agonism, and molecular modelling suggested that the hydrogen bond acceptors of these groups lie approximately at the same distances from each other as the amide and *N*-sulfonyl anilide groups in the biphenyl scaffold of **Nag 26**. In this study, we use azulene as a substitute for the biphenyl moiety of **Nag 26** to further study the applicability of azulenes as biphenyl mimetics in orexin receptor ligands. The effect of replacing the biphenyl moiety of **Nag 26** with a fused bicyclic aromatic structure on orexin receptor activity is reported for the first time.

2. Results and discussion

We synthesized azulene derivatives from two building blocks, A and B, which are suitable for sulfonamide coupling in the end of the synthesis (Figure 1). Building block A is a 1-sulfonate azulene with the 3- and 6-positions available for functionalization and building block B is the unmodified half of **Nag 26**.

6-Methylazulene (**7**)[27] or the 6-carboxyazulene[25]-derived amide **8** were used as starting compounds for synthesis of building block A and the synthesis was started by introducing a trifluoroacetyl or a dimethylamide functionality into position 1 (Scheme 1b). The trifluoroacetyl group was introduced with trifluoroacetic anhydride (TFAA) in the presence of Et_3N giving **9** and **11** in 83% and 94% yields, respectively. The dimethylamide derivative **12** was obtained in 60% yield upon heating **8** and phosgene in toluene followed by addition of dimethylamine.[26] To obtain **10**, the temperature was lowered and reaction time shortened, as heating the reaction mixture led to an insoluble solid. The optimized reaction resulted in **10** in 76% yield.

Introduction of a sulfonic acid group to the non-functionalized five-membered ring of azulene failed to give the monosubstituted product, as only the 1,3-disulfonic acid derivative and unreacted starting material were obtained. However, the sulfonic acid derivatives with dimethylamide or trifluoroacetyl group in the 3-position were obtained as sodium sulfonates in good yields. Altogether four different A building blocks, **13**, **14**, **15** and **16**, were synthesized.

The synthesis of the building block B (compound **20**) was started by heating 1-fluoro-3-nitrobenzene (**17**) in ethylenediamine, which was followed by the addition of toluoyl chloride to give **18** (Scheme 1c). In order to avoid selectivity issues in the coupling of the building blocks A and B, the amino group of **18** was protected with trifluoroacetamide using TFAA. The reduction of the nitro group of **19** gave **20** in 27% yield over three steps.

Building blocks A and B were combined by first converting the sulfonate groups of **13**–**16** to sulfonyl chlorides by heating them in $SOCl_2$ (Scheme 1a). Then, the reaction between the sulfonyl chlorides and compound **20** gave **21**–**24** in 31%, 44%, 38% and 18% yields, respectively. The compounds were deprotected with K_2CO_3 in water and methanol to give the final products **25**, **27**, **28** and **29** in 39%, 53%, 76% and 40% yield, respectively.

As the building block B is the unmodified half of **Nag 26**, it is a useful intermediate also in the synthesis of **Nag 26,** which was synthesized from **20** in two steps with 30% yield. First, **20** was reacted with 5-bromo-2-methoxybenzenesulfonylchloride to give the sulfonamide **30**. Dimethylaminocarbonyl benzene moiety was coupled to **30** under Suzuki reaction conditions with simultaneous deprotection of the amine to obtain **Nag 26**. This route reduces the required synthetic steps from eleven to six compared to the original route for **Nag 26**. Pharmacological characterization of the resulting **Nag 26** has been reported previously.[22]

OX_1 and OX_2 receptor activation was evaluated first for four azulene-based analogs of **Nag 26** and eight synthesis intermediates by measuring compound-mediated Ca^{2+} elevation at 10 μM compound concentration in three independent experiments (Supporting Information Figure S1). Two compounds induced OX_1-mediated Ca^{2+} elevation, **27** with 80 ±

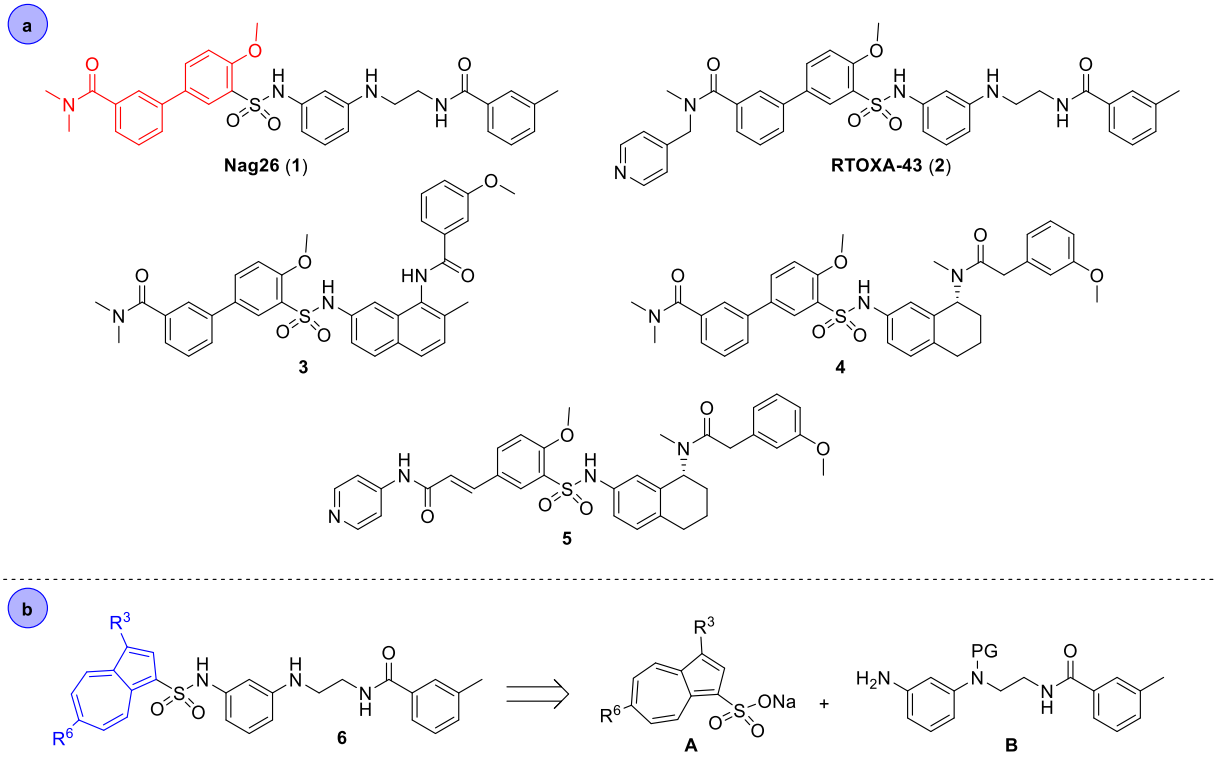

Figure 1. a. Small molecule orexin receptor agonists. **b.** Azulene derivatives (in blue) were designed to replace the biphenyl structure of **Nag 26** (in red). The synthesis of the azulene-based compounds was designed from building blocks A and B.

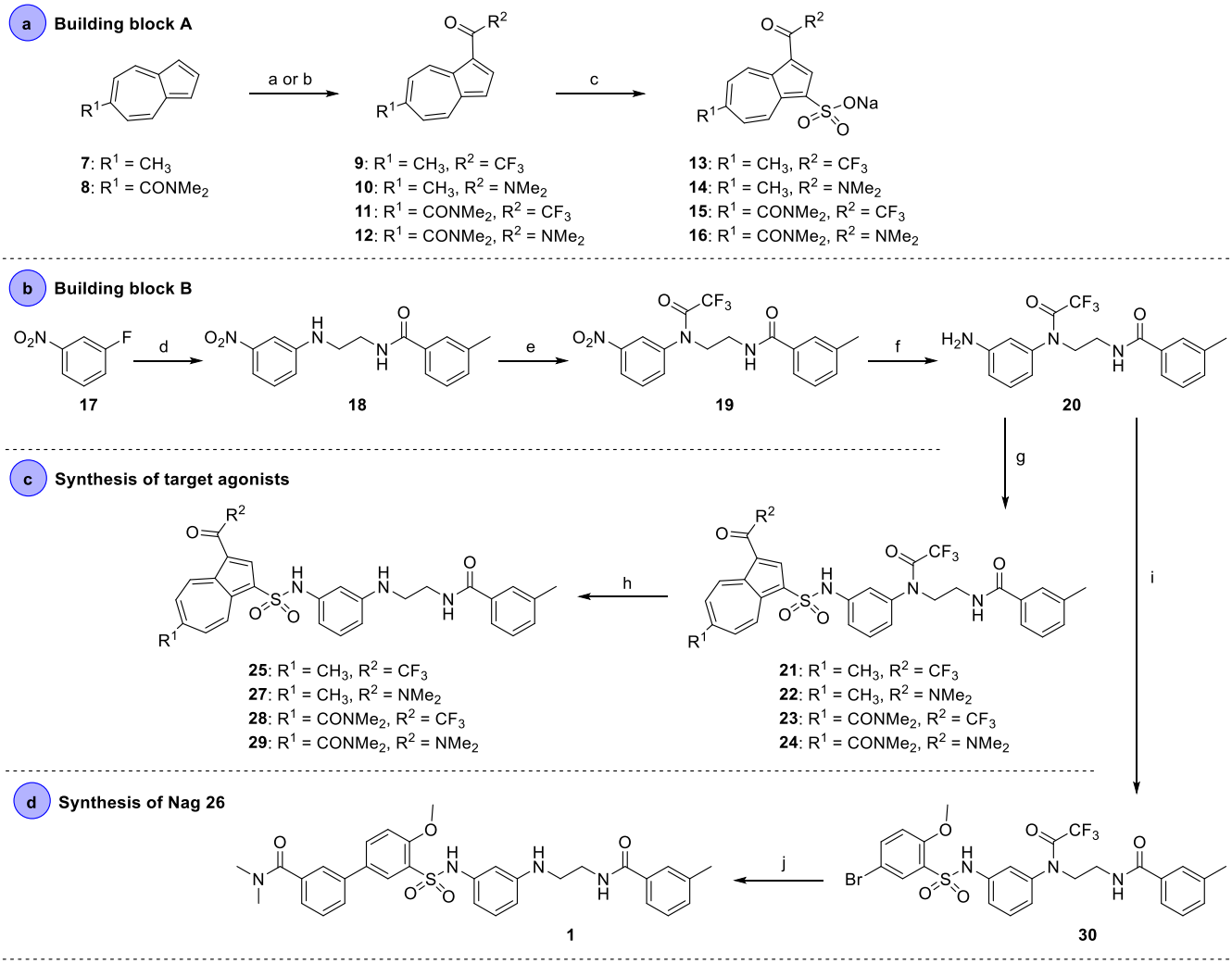

Scheme 1. Synthesis of azulene-based target agonists via building blocks A and B, and a novel synthetic route for **Nag 26**. Reagents and conditions: (a) TFAA, Et_3N, DCM, 0 °C, 1 h, 83% (**9**), 94% (**11**); (b) i) Phosgene, toluene, rt or 80 °C, 1.5–5.5 h, ii) Dimethylamine, THF, 0 °C, 30 min, 76% (**10**), 60% (**12**); (c) i) Sulfur trioxide pyridine complex, benzene, 85 °C, 3.5 h, ii) NaOH, H_2O, EtOH, 30 °C, 2 h, 84% (**13**), 88% (**14**), 53% (**15**), 77% (**16**); (d) i) Ethylenediamine, 100 °C, 23 h, ii) *m*-Toluoyl chloride, *N*,*N*-diisopropylethylamine (DIPEA), DCM, 0 °C, 2 h, 54%; (e) TFAA, Et_3N, THF, 0 °C, 1 h, 99%; (f) H_2, Pd/C, EtOH, rt, 4.5 h, 51%; (g) i) Building block A, $SOCl_2$, 67 °C, 15 min, ii) **20**, Et_3N, DCM, rt, 19–22 h, 31% (**21**), 44% (**22**), 38% (**23**), 18% (**24**); (h) K_2CO_3, MeOH, H_2O, rt, 3 h, 39% (**25**), 53% (**27**), 76% (**28**), 40% (**29**); (i) 5-Bromo-2-methoxybenzenesulfonyl chloride, Et_3N, DCM, rt, 48 h, 57%; (j) 3-(*N*,*N*-Dimethylaminocarbonyl)benzeneboronic acid, Pd(dppf)Cl_2, Na_2CO_3, H_2O, 1,4-dioxane, 100 °C, 48 h, 53%.

7% and **29** with 11 ± 4% of the maximum response to orexin-A (Supporting Information Figure S1), while none of the compounds induced Ca^{2+} response via OX_2 receptors. To further confirm that the observed responses were indeed OX_1-mediated, we repeated the measurements using control CHO cells that do not express OX_1 receptors; no response to **27** and **29** were observed on these cells (Supporting Information Figure S2). Subsequently, we studied the ability of these 12 compounds to block the orexin-A-induced Ca^{2+} signal (Supporting Information Figure S3). Compound **27** was showing OX_1 and OX_2 antagonism corresponding to ca. 4 μM and 2 μM K_i values, respectively. However, as **27** also showed efficacy on OX_1, the K_i estimate on OX_1 might be misleading. On OX_2, also **24**, **25** and **29** blocked the response to 0.3 nM orexin-A at levels corresponding to approximately 5–10 μM K_i. The rest of the compounds had only a minor effect on the orexin-A response indicating $K_i > 10$ μM if any.

We continued with **27** assessing the concentration-dependence of the Ca^{2+} elevation on OX_1 receptors; stimulation by **27** led to a similar magnitude of Ca^{2+} elevation as by orexin-A, but with a notably weaker potency (Figure 2). Furthermore, the effect of **27** is approximately 10% of the effect of **Nag 26** on OX_1-receptors; pEC_{50} for **27** was 5.79 ± 0.07 (n = 5) and for **Nag 26** 6.66 ± 0.06 (as measured previously with identical assay set-up.[22] However, OX_2 activation differs dramatically between these two compounds – **Nag 26** is also a potent OX_2 agonist (pEC_{50} = 7.77 ± 0.07[22]), whereas **27** has no OX_2 activity (Supporting Information Figure S1).

To explain further the observed preference in efficacy of **27** towards OX_1 receptor compared to OX_2, and corresponding structure–activity relationships, we took an advantage of a recently published cryo-EM structure of OX_2 in complex with a G protein and a small molecule agonist **31** (PDB ID: 7L1V), structurally closely related to **Nag 26** (Figure 3).[28] OX_2 shares 80% sequence identity with OX_1 in the TM region and has nearly identical ligand binding site (only 2–4 differing amino acid residues, depending on how the binding site is framed). We built a homology model of OX_1 based on the cryo-EM structure of OX_2 and docked **27** to the OX_1 model; the conformation and the interactions formed by the highest scoring binding mode of **27** were similar to those of **31** in the OX_2 structure (Figure 3 a and b).

In the **27** docking pose, the sulfonamide core of **27** forms two hydrogen bonds with the upward-facing $Gln^{3.32}$ (for the amino acid numbering, see references[29,30]), while the surrounding ring structures

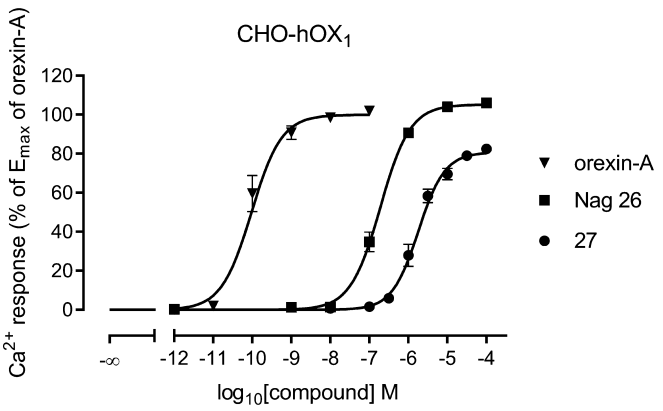

Figure 2. Ca^{2+} responses to orexin-A (filled triangles), **Nag 26** (filled squares) and **27** (filled circles) on CHO-hOX_1 cells. The responses were normalized to baseline separately for each independent sample before averaging. N = 5. **Nag 26** graph is reproduced from data originally published by Rinne *et al.*[22] for easier comparison.

are lined by $Pro^{3.29}$, $Met^{4.64}$, $Ser^{2.61}$ and $Val^{2.64}$. The ability to stabilize $Gln^{3.32}$ in the upward conformation was shown to be crucial for agonist activity on OX_2 receptors.[28] Notably, only compounds with a sulfonamide group have been reported as potent small molecule orexin receptor agonists so far.[16–21] The hydrophobic bottom of the binding cavity is occupied by the amide-linked tolyl, while the amide carbonyl lays within a hydrogen-bonding distance from $His^{7.39}$. Compounds with the trifuoroacetyl protecting group of the secondary amine (as in **22** and **24**) were inactive, suggesting that limited space is available in the bottom of the binding site.

The azulene moiety of **27** is located near TM2 and TM7, surrounded by residues $His^{7.39}$, $Tyr^{7.32}$, $Val^{2.64}$, and $Ser^{2.61}$. The methyl group in the 6-position of the azulene occupies a nook between $Ser^{2.61}$ and $His^{7.39}$. $Ser^{2.61}$ is one of the few positions where the ligand binding site of OX_1 differs from that of OX_2; OX_2 has a threonine in this position, thus leaving less room between TM2 and TM7. This likely explains the difference between the orexin receptor subtypes in efficacy of **27**, as the methyl group would not fit between TM2 and TM7 in OX_2 as it does in OX_1 (Figure 3c). Furthermore, when replacing the methyl group in the 6-position of azulene with a dimethylamide group (compound **29**), the OX_1 agonist activity decreases dramatically, as there is likely no room for a larger functional group between the helices. Even more drastic drop in the activity is observed when the dimethylamide group in the 3-position of azulene was replaced with a trifluoroacetyl group, as both trifluoroacetyl derivatives **25** and **28** were inactive.

Previously reported modifications at a certain position of **Nag 26** structure have resulted in either OX_2 selective agonists, or agonists with equal effect on both orexin receptors.[19–21] Identification of OX_1 selectivity has required the modification of the structure of **Nag 26** on both ends of the molecule – at first, a tetralin-type dual-orecin receptor agonist **4** was developed,[21] and further replacement of the biphenyl structure of **4** with anisole or cinnamide derivative has led to compounds preferentially activating OX_1 at moderate potency.[23] Optimization of the compounds has resulted in the first potent OX_1 selective agonist **5**. Interestingly, replacing the biphenyl moiety of **Nag 26** itself with cinnamide derivative has led to complete loss of both OX_1 and OX_2 activity,[19] suggesting that the preference towards OX_1 in compound **5** and its analogs is not dependent solely on the modification of the biphenyl structure. Thus, the azulene-based derivative **27** reported herein is the first analog of **Nag 26** with preference towards OX_1, which has been reached by modifying only the biphenyl structure. As such, compound **27** contributes to the establishment of structure–activity relationships related to subtype selectivity between the orexin receptors and development of OX_1-selective agonists, although the potency of the compound has yet remained moderate.

3. Conclusions

In conclusion, our results demonstrate that the azulene ring can mimic a biphenyl moiety in orexin receptor agonists. Both types of orexin receptor agonists, those bearing biphenyl as well as those bearing

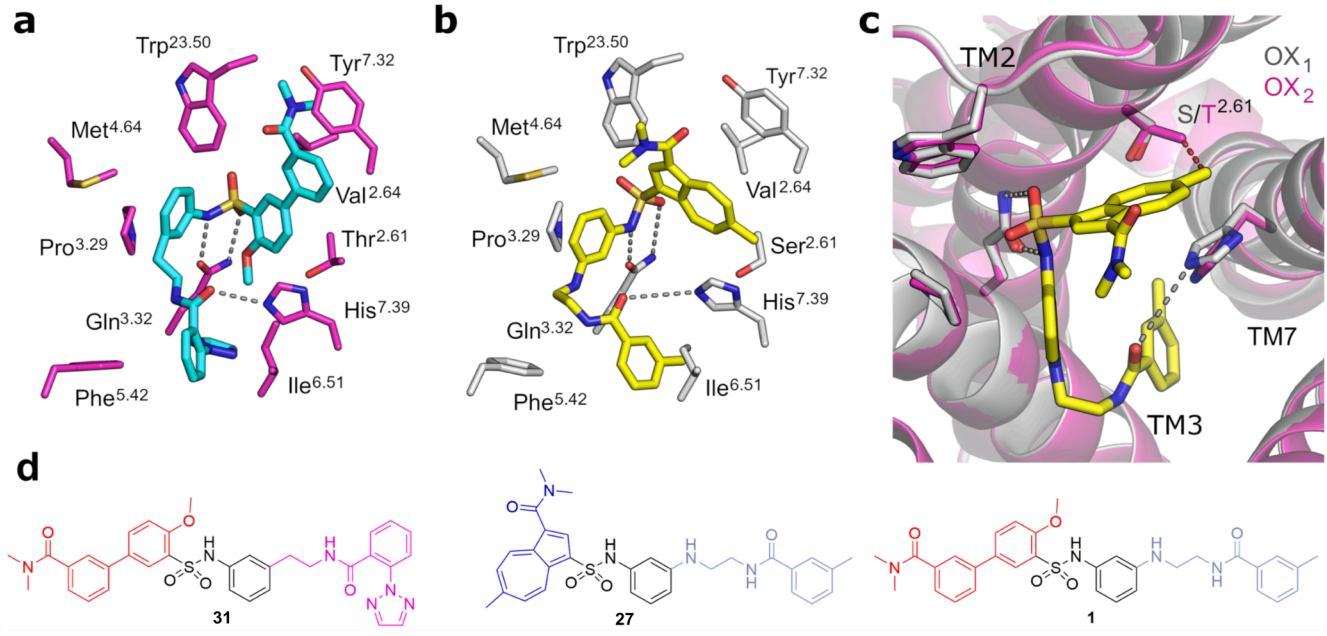

Figure 3. a. Binding mode of agonist **31** (cyan) in complex with OX_2 (PDB ID: 7L1V). **b.** Docking pose of **27** (bright yellow) in complex with OX_1 homology model. **c.** Superimposition of **27**-OX_1 complex to OX_2 structure. Red dashes mark the possible clash between **27** and OX_2. Receptors are shown as cartoon and the binding site residues as sticks (white and pink for OX_1 and OX_2, respectively). Color code is as follows: blue, nitrogen; red, oxygen; yellow, sulfur; pink (OX_2) / white (OX_1) / cyan (**31**) / bright yellow (**27**), carbon. Gray dashes indicate possible hydrogen bonds. **d.** 2D comparison of **Nag 26** (**1**), **27** and **31**. Analogous parts of the compounds are marked with same colors.

azulene scaffold, have been shown to exhibit good efficacy on orexin receptors. While the efficacy of the azulene-based OX_1 agonist **27** is close to that of orexin-A, the potency of **27** remains moderate. However, this study was based on a limited number of compounds, and thus further compound optimization could improve the potency. As the majority of the currently known small molecule orexin receptor agonists are OX_2-selective, **27** poses a promising starting point for developing OX_1-selective tool compounds for pharmacological research to validate the significance of OX_1 modulation *in vivo*. Understanding the structure–activity relationships for OX_1-selective agonists could also open other therapeutic opportunities in conditions such as colon cancer.

4. Experimental section

4.1. Chemistry

General information: All compounds were characterized by NMR spectroscopy using a Bruker Avance III 400 MHz spectrometer or a Varian Mercury 300 MHz spectrometer. Chemical shifts are reported in parts per million (ppm) relative to the residual solvent signals: $CDCl_3$ 7.26 and 77.16 ppm, DMSO-d_6 2.50 and 39.52 ppm, acetone-d_6 2.05 and 29.84 ppm, CD_3OD 3.31 and 49.00 ppm for ^1H and ^{13}C NMR, respectively. The progress of the reactions was monitored by thin-layer chromatography on silica gel 60-F_{254} plates. When a product was purified by flash chromatography, silica gel (SiO_2) 60 (230–400 mesh) or silica gel with a Biotage SP1 purification system (SNAP 10, 25, or 50 g cartridges) was used. Mass spectrometric analysis were performed with a Waters Synapt G2 HDMS mass spectrometer using electrospray ionization (ESI). The purity was determined by UPLC-MS with diode-array detector. The purity of all biologically tested compounds was 95% or higher.

***N,N*-Dimethylazulene-6-carboxamide (8).** Azulene-6-carboxylic acid (0.25 g, 1.4 mmol) was dissolved in DMF (5.5 mL). The blue solution was cooled to 0 °C and EDC·HCl (0.30 g, 1.6 mmol) and HOBt·H_2O (0.24 g, 1.6 mmol) were added. The reaction mixture was stirred at 0 °C for 15 min and at room temperature for 1 h. A 2 M solution of dimethylamine in THF (1.8 mL, 3.6 mmol) was added and the stirring was continued at room temperature for 1 h. H_2O (40 mL) was added to the reaction mixture, and it was extracted with EtOAc (80 mL). The organic phase was washed with a 1 M aqueous solution of HCl (40 mL) and a saturated aqueous solution of $NaHCO_3$ (40 mL), dried over anhydrous Na_2SO_4, filtered, and evaporated to provide a green solid. The crude product was purified by flash chromatography (EtOAc) to give **8** as a green, amorphous solid (0.23 g, 81%). ^1H NMR (400 MHz, $CDCl_3$) δ 8.39–8.36 (m, 2H), 7.97–7.96 (m, 1H), 7.45–7.44 (m, 2H), 7.15–7.12 (m, 2H), 3.16 (s, 3H), 2.94 (s, 3H). ^{13}C NMR (101 MHz, $CDCl_3$) δ 172.9, 144.9, 140.1, 138.5, 136.3, 120.8, 119.4, 39.5, 35.4. HRMS (ESI-QTOF) *m/z*: $[M + H]^+$ Calcd for $C_{13}H_{14}NO$ 200.1075; Found 200.1077.

2,2,2-Trifluoro-1-(6-methylazulen-1-yl)ethan-1-one (9). TFAA (0.46 mL, 3.3 mmol) was added dropwise to a solution of 6-methylazulene (0.43 g, 3.0 mmol) and Et_3N (0.84 mL, 6.0 mmol) in anhydrous DCM (8.0 mL) under argon on ice bath. The resulting mixture was stirred at 0 °C for 1 h. Then H_2O (60 mL) was added and stirring was continued for an additional 5 min. DCM (60 mL) was added and phases were separated. The organic phase was washed with H_2O (3 × 40 mL) and brine (40 mL), dried over anhydrous Na_2SO_4, filtered, and evaporated to provide a red solid. The crude product was purified by flash chromatography (*n*-heptane/EtOAc 9:1) to give **9** as a red, amorphous solid (0.60 g, 83%). ^1H NMR (300 MHz, $CDCl_3$) δ 9.72 (d, J = 10.2 Hz, 1H), 8.39 (d, J = 10.2 Hz, 1H), 8.26–8.23 (m, 1H), 7.67 (d, J = 10.5 Hz, 1H), 7.57 (d, J = 10.2 Hz, 1H), 7.23 (d, J = 4.2 Hz, 1H), 2.78 (s, 3H). ^{13}C NMR (75 MHz, $CDCl_3$) δ 176.0 (q, J = 33.5 Hz), 153.6, 146.0, 142.7, 139.8 (q, J = 3.8 Hz), 138.9, 138.2, 133.0, 131.9, 119.6, 117.6, 117.6 (q, J = 290.2 Hz), 28.3. HRMS (ESI-QTOF) *m/z*: $[M + H]^+$ Calcd for $C_{13}H_{10}OF_3$ 239.0684; Found 239.0690.

***N,N*,6-Trimethylazulene-1-carboxamide (10).** A 20% solution of phosgene in toluene (9.3 mL, 18 mmol) was added to a solution of 6-methylazulene (0.50 g, 3.5 mmol) in anhydrous toluene (0.90 mL) under argon. The resulting dark blue solution was stirred at room temperature for 1.5 h and then solvents were evaporated. The purple residue was dissolved in anhydous THF (6.0 mL) under argon. The purple solution was cooled to 0 °C and a 2 M solution of dimethylamine in THF (8.8 mL) was slowly added. The reaction mixture was stirred at 0 °C for 30 min. The mixture was diluted with DCM (60 mL) and washed with a 1 M aqueous solution of HCl (30 mL). The aqueous phase was extracted with DCM (3 × 60 mL + 1 × 30 mL). The organic phases were combined, washed with a saturated aqueous solution of $NaHCO_3$ (100 mL) and H_2O (100 mL), dried over anhydrous Na_2SO_4, filtered, and evaporated to provide a purple oil. The crude product was purified by flash chromatography (*n*-heptane/EtOAc 1:4) to give **10** as a purple oil (0.57 g, 76%). ^1H NMR (400 MHz, $CDCl_3$) δ 8.62 (d, J = 10.0 Hz, 1H), 8.25 (d, J = 10.0 Hz, 1H), 7.82 (d, J = 4.0 Hz, 1H), 7.25–7.19 (m, 3H), 3.15 (s, 6H), 2.67 (s, 3H). ^{13}C NMR (101 MHz, $CDCl_3$) δ 169.4, 150.7, 140.6, 137.0, 136.9, 136.1, 135.5, 126.8, 126.4, 122.8, 116.7, 37.6* 28.3 (*Methyl carbons of amide only visible in HSQC). HRMS (ESI-QTOF) *m/z*: $[M + H]^+$ Calcd for $C_{14}H_{16}NO$ 214.1232; Found 214.1233.

***N,N*-Dimethyl-1-(2,2,2-trifluoroacetyl)azulene-6-carboxamide (11).** TFAA (0.30 mL, 2.3 mmol) was added dropwise to a solution of **8** (0.15 g, 0.75 mmol) and Et_3N (0.32 mL, 2.3 mmol) in anhydrous DCM (2.1 mL) under argon on ice bath. The resulting mixture was stirred at 0 °C for 1 h. Then H_2O (15 mL) was added and stirring was continued for an additional 5 min. DCM (45 mL) was added and phases were separated. The organic phase was washed with H_2O (2 × 30 mL) and brine (30 mL), dried over anhydrous Na_2SO_4, filtered, and evaporated to provide a purple solid. The crude product was purified by flash chromatography (*n*-heptane/EtOAc 2:3) to give **11** as purple, amorphous solid (0.21 g, 94%). ^1H NMR (400 MHz, $CDCl_3$) δ 9.87 (d, J = 10.4 Hz, 1H), 8.58 (d, J = 10.0 Hz, 1H), 8.42–8.40 (m, 1H), 7.72 (dd, J = 10.2 Hz, 1.4 Hz, 1H), 7.63 (dd, J = 10.0 Hz, 1.6 Hz, 1H) 7.38 (d, J = 4.4 Hz, 1H), 3.20 (s, 3H), 2.95 (s, 3H). ^{13}C NMR (101 MHz, $CDCl_3$) δ 176.2 (q, $^2J_{C,F}$ = 34.3 Hz), 171.0, 148.3, 146.8, 143.6, 142.2 (q, $^3J_{C,F}$ = 3.7 Hz), 139.3, 139.1, 129.1, 128.0, 120.7, 118.3, 117.4 (q, $^1J_{C,F}$ = 292.9 Hz), 39.5, 35.5. HRMS (ESI-QTOF) *m/z*: $[M + H]^+$ Calcd for $C_{15}H_{13}NO_2F_3$ 296.0898; Found 296.0901.

***N*^{1},*N*^{1},*N*^{6},*N*^{6}-Tetramethylazulene-1,6-dicarboxamide (12).** A 20% solution of phosgene in toluene (1.7 mL, 3.3 mmol) was added to a solution of **8** (0.13 g, 0.65 mmol) in anhydrous toluene (5.0 mL) under argon. The resulting dark blue solution was heated at 80 °C for 5.5 h and then solvents were evaporated. The purple residue was dissolved in anhydous THF (1.1 mL) under argon. The purple solution was cooled to 0 °C and a 2 M solution of dimethylamine in THF (1.6 mL) was slowly added. The reaction mixture was stirred at 0 °C for 30 min. The mixture was diluted with DCM (30 mL) and washed with a 1 M aqueous solution of HCl (15 mL), a saturated aqueous solution of $NaHCO_3$ (15 mL) and H_2O (15 mL), dried over anhydrous Na_2SO_4, filtered, and evaporated to provide a dark blue solid. The crude product was purified by flash chromatography (manual gradient of EtOAc → EtOAc/MeOH 97:3) to give **12** as a dark blue, amorphous solid (0.11 g, 60%). ^1H NMR (400 MHz, $CDCl_3$) δ 8.74 (d, J = 10.0 Hz, 1H), 8.40 (d, J = 10.0 Hz, 1H), 7.97 (d, J = 3.6 Hz, 1H), 7.35 (d, J = 4.0 Hz, 1H), 7.26–7.24 (m, 2H), 3.16 (m, 9H), 2.92 (s, 3H). ^{13}C NMR (101 MHz, $CDCl_3$) δ 172.3, 168.8, 146.2, 141.7, 137.9, 137.9, 137.6, 136.6, 124.3, 122.9, 122.7, 118.0, 39.5, 35.4. HRMS (ESI-QTOF) *m/z*: $[M + H]^+$ Calcd for $C_{16}H_{19}N_2O_2$ 271.1447; Found 271.1447.

General procedure for the synthesis of compounds 13, 14, 15, 16. A mixture of the appropriate azulene derivative and sulfur trioxide pyridine complex (3 equiv) in anhydrous benzene (1.5–10 mL) under argon was heated at 85 °C for 3.5 h. Solvents were evaporated and the residue was dissolved in EtOH (2.2–15 mL). A 1 M aqueous solution of NaOH (2.2–15 mL) was added and the resulting mixture was stirred at 30 °C for 2 h. *n*-Butanol and brine were added to the reaction mixture. Phases were separated and the aqueous phase was extracted with several

times of *n*-butanol. The organic phases were combined and dried over anhydrous Na_2SO_4, filtered and evaporated to provide a crude product, which was purified by flash chromatography.

Sodium 6-methyl-3-(2,2,2-trifluoroacetyl)azulene-1-sulfonate (13). Compound **9** (0.48 g, 2.0 mmol) gave a red solid, which after flash chromatography (manual gradient of MeCN/EtOH 9:1 → 3:2) yielded **13** as a pink, amorphous solid (0.57 g, 84%). ^{1}H NMR (400 MHz, CD_3OD) δ 9.79 (d, $J = 10.4$ Hz, 1H), 9.30 (d, $J = 10.8$ Hz, 1H), 8.49–8.48 (m, 1H), 7.97–7.94 (m, 2H), 2.86 (s, 3H). ^{13}C NMR (101 MHz, CD_3OD) δ 176.7 (q, $J = 33.8$ Hz), 158.1, 145.0, 141.6, 140.9, 140.0, 139.6 (q, $J = 3.9$ Hz), 136.0, 135.1, 134.3, 118.7 (q, $J = 292.5$ Hz), 114.9, 28.2. HRMS (ESI-TOF) *m/z*: $[M - Na]^-$ Calcd for $C_{13}H_8O_4F_3S$ 317.0096; Found 317.0099.

Sodium 3-(dimethylcarbamoyl)-6-methylazulene-1-sulfonate (14). Compound **10** (0.54 g, 2.5 mmol) gave a purple solid, which after flash chromatography (manual gradient of MeCN/EtOH 4:1 → 3:2) yielded **14** as a purple, amorphous solid (0.70 g, 88%). ^{1}H NMR (400 MHz, CD_3OD) δ 9.15 (d, $J = 10.0$ Hz, 1H), 8.59 (d, $J = 10.4$ Hz, 1H), 8.10 (s, 1H), 7.57–7.54 (m, 1H), 7.52–7.49 (m, 1H), 3.15 (s, 6H), 2.75 (s, 3H). ^{13}C NMR (101 MHz, CD_3OD) δ 170.6, 154.7, 139.3, 138.6, 138.2, 136.2, 135.8, 131.1, 129.9, 129.7, 120.8, 40.1, 35.8, 28.2. HRMS (ESI-QTOF) *m/z*: $[M - Na + 2H]^+$ Calcd for $C_{14}H_{16}NO_4S$ 294.0800; Found 294.0800.

Sodium 6-(dimethylcarbamoyl)-3-(2,2,2-trifluoroacetyl)azulene-1-sulfonate (15). Compound **11** (0.23 g, 0.78 mmol) gave a red solid, which after flash chromatography (manual gradient of MeCN → MeCN/EtOH 4:1) yielded **15** as a red, amorphous solid (0.16 g, 53%). ^{1}H NMR (400 MHz, CD_3OD) δ 9.98 (d, $J = 10.4$ Hz, 1H), 9.51 (d, $J = 10.4$ Hz, 1H), 8.67–8.65 (m, 1H), 7.98–7.93 (m, 2H), 3.19 (s, 3H), 2.97 (s, 3H). HRMS (ESI-QTOF) *m/z*: $[M - Na + 2H]^+$ Calcd for $C_{15}H_{13}NO_5F_3S$ 376.0467; Found 376.0466.

Sodium 3,6-bis(dimethylcarbamoyl)azulene-1-sulfonate (16). Compound **12** (0.099 g, 0.37 mmol) gave a blue solid, which after flash chromatography (MeCN/EtOH 8:2) yielded **16** as a blue, amorphous solid (0.11 g, 77%). ^{1}H NMR (400 MHz, CD_3OD) δ 9.34 (d, $J = 10.0$ Hz, 1H), 8.76 (d, $J = 10.0$ Hz, 1H), 8.27 (s, 1H), 7.55–7.52 (m, 1H), 7.49–7.47 (m, 1H), 3.19–3.14 (m, 9H), 2.96 (s, 3H). ^{13}C NMR (101 MHz, CD_3OD) δ 173.5, 170.0, 148.7, 140.3, 139.3, 139.1, 138.3, 137.2, 132.9, 125.8, 125.7, 122.6, 39.7, 35.5. HRMS (ESI-QTOF) *m/z*: $[M - Na + 2H]^+$ Calcd for $C_{16}H_{19}N_2O_5S$ 351.1015; Found 351.1015.

3-Methyl-*N*-[2-[(3-nitrophenyl)amino] ethyl] benzamide (18). A mixture of 1-fluoro-3-nitrobenzene (1.1 mL, 10 mmol) and ethylenediamine (7.5 mL) was heated at 100 °C for 23 h under argon. The red reaction mixture was quenched with a saturated aqueous solution of $NaHCO_3$ (70 mL) and it was extracted with DCM (3 × 40 mL). The organic phases were combined, washed with brine (2 × 50 mL), dried over anhydrous Na_2SO_4, filtered, and evaporated to provide a red solid. The solid was dissolved in anhydrous DCM (40 mL) under argon and DIPEA (3.2 mL, 19 mmol) was added. The resulting mixture was cooled to 0 °C and *m*-toluoyl chloride (1.2 mL, 9.3 mmol) was added dropwise over 5 min. The reaction mixture was stirred at 0 °C for 2 h and then it was diluted with DCM (40 mL). The organic phase was washed with a saturated aqueous solution of $NaHCO_3$ (3 × 40 mL) and brine (30 mL), dried over anhydrous Na_2SO_4, filtered, and evaporated to provide an orange solid. The crude product was purified by flash chromatography (*n*-heptane/(EtOAc:EtOH 3:1) 1:1 → 2:3) to give **18** as a yellow, amorphous solid (1.6 g, 54%). ^{1}H NMR (400 MHz, acetone-d_6) δ 7.96 (s, 1H), 7.70–7.65 (m, 2H), 7.45 (t, $J = 2.2$ Hz, 1H), 7.42–7.39, (m, 1H), 7.35–7.31 (m, 3H), 7.10–7.07 (m, 1H), 5.94–5.90 (m, 1H), 3.69–3.64 (m, 2H), 3.50–3.45 (m, 2H), 2.36 (s, 3H). ^{13}C NMR (101 MHz, acetone-d_6) δ 168.2, 150.9, 150.4, 138.8, 135.8, 132.6, 130.8, 129.1, 128.6, 125.1, 119.1, 111.2, 106.4, 44.0, 39.7, 21.31. HRMS (ESI-QTOF) *m/z*: $[M + H]^+$ Calcd for $C_{16}H_{18}N_3O_3$ 300.1348; Found 300.1351.

3-Methyl-*N*-[2-[2,2,2-trifluoro-*N*-(3-nitrophenyl)acetamido] ethyl] benzamide (19). TFAA (0.75 mL, 5.4 mmol) was added dropwise over 5 min to a solution of **18** (1.6 g, 5.4 mmol) and Et_3N (0.75 mL, 5.4 mmol) in anhydrous THF (36 mL) under argon on ice bath. The resulting mixture was stirred at 0 °C for 1 h. A 1 M aqueous solution of HCl (60 mL) was added and the resulting suspension was stirred at 0 °C for 20 min. The reaction mixture was extracted with DCM (100 mL). The phases were separated and the organic phase was washed with H_2O (60 mL) and brine (60 mL), dried over anhydrous Na_2SO_4, filtered and evaporated to provide a brownish solid. The crude product was purified by flash chromatography (DCM/MeOH 99:1 → 9:1) to give **19** as a yellow, amorphous solid (2.1 g, 99%). ^{1}H NMR (400 MHz, ($CDCl_3$) δ 8.30 (d, $J = 8.4$ Hz, 1H), 8.23–8.22 (m, 1H), 7.75–7.73 (m, 1H), 7.67–7.63 (m, 1H), 7.55 (s, 1H), 7.51–7.48 (m, 1H), 7.32–71 (m, 2H), 6.66 (s, 1H), 4.11–4.06 (m, 2H), 3.76–3.75 (m, 2H), 2.39 (s, 3H). ^{13}C NMR (101 MHz, $CDCl_3$) δ 168.4, 157.9 (q, $^2J_{C,F} = 36.9$ Hz), 148.9, 140.2, 138.8, 134.9, 133.8, 132.8, 130.8, 128.7, 127.8, 124.5, 123.9, 123.6, 116.1 (q, $^1J_{C,F} = 289.3$ Hz), 51.4, 38.0, 21.5. HRMS (ESI-QTOF) *m/z*: $[M + H]^+$ Calcd for $C_{18}H_{17}N_3O_4F_3$ 396.1171; Found 396.1171.

***N*-[2-[*N*-(3-Aminophenyl)-2,2,2-trifluoroacetamido] ethyl]-3-methylbenzamide (20).** Compound **19** (2.1 g, 5.3 mmol) was dissolved in EtOH (45 mL) and Pd/C (0.21 g) was added. The resulting black mixture was stirred under H_2 at room temperature for 4 h. The reaction mixture was filtered through a small pad of Celite with EtOH. Solvents were evaporated to provide a yellow solid. After two flash chromatographic purifications (*n*-heptane/(EtOAc:EtOH 3:1) 9:1 → 2:3 and DCM/MeOH 99:1 → 19:1) **20** was obtained as yellow, amorphous solid (1.0 g, 51%). ^{1}H NMR (400 MHz, $CDCl_3$) δ 7.58 (s, 1H), 7.53–7.51 (m, 1H), 7.31–7.30 (m, 2H), 7.17 (t, $J = 8.0$ Hz, 1H), 6.80–6.78 (m, 1H), 6.70–6.68 (m, 1H), 6.61–6.60 (m, 1H), 6.56–6.55 (m, 1H), 4.02–3.99 (m, 2H), 3.74–3.70 (m, 2H), 2.39 (s, 3H). ^{13}C NMR (101 MHz, $CDCl_3$) δ 168.1, 158.6 (q, $^2J_{C,F} = 36.2$ Hz), 147.9, 139.8, 138.6, 134.1, 132.5, 130.5, 128.7, 127.9, 123.9, 117.6, 116.5 (q, $^1J_{C,F} = 289.1$ Hz), 115.9, 114.2, 51.0, 38.8, 21.5. HRMS (ESI-QTOF) *m/z*: $[M + H]^+$ Calcd for $C_{18}H_{19}N_3O_2F_3$ 366.1429; Found 366.1429.

General procedure for the synthesis of compounds 21, 22, 23, 24. A mixture of the appropriate azulene derivative (1–2 equiv) and $SOCl_2$ (0.80–2.0 mL) was heated at 67 °C for 15 min. $SOCl_2$ was evaporated and the residue was dissolved in anhydrous DCM (1–5 mL) under argon. Compound **20** (1 equiv) and Et_3N (4 equiv) were added, and the resulting mixture was stirred at room temperature for 19–22 h. A 1 M aqueous solution of HCl (5.0–10 mL) was added and then the mixture was stirred for 5 min. The mixture was diluted with DCM (15–50 mL) and the organic phase was washed with a 1 M aqueous solution of HCl (3 × 10–50 mL) and brine (10–50 mL), dried over anhydrous Na_2SO_4, filtered, and evaporated to provide a crude product, which was purified by flash chromatography.

3-Methyl-*N*-[2-[2,2,2-trifluoro-*N*-[3-[[6-methyl-3-(2,2,2-trifluoroacetyl)azulene]-1-sulfonamido] phenyl] acetamido] ethyl] benzamide (21). Compound **13** (0.20 g, 0.60 mmol) and **20** (0.11 g, 0.30 mmol) gave a dark red solid, which after flash chromatography (DCM/MeOH 99:1) yielded **21** as an orange, amorphous solid (0.062 g, 31%). ^{1}H NMR (400 MHz, acetone-d_6) δ 9.80 (d, $J = 10.4$ Hz, 1H), 9.42 (s, 1H), 9.20 (d, $J = 10.4$ Hz, 1H), 8.45–8.43 (m, 1H), 8.15 (d, $J = 10.8$ Hz, 1H), 8.09 (d, $J = 10.4$ Hz, 1H), 7.76–7.72 (m, 1H), 7.57–7.53 (m, 2H), 7.31–7.22 (m, 6H), 3.84 (t, $J = 5.6$ Hz, 2H), 3.47–3.43 (m, 2H), 2.89 (s, 3H), 2.35 (s, 3H). HRMS (ESI-QTOF) *m/z*: $[M + H]^+$ Calcd for $C_{31}H_{26}N_3O_5F_6S$ 666.1497; Found 666.1497.

***N,N*,6-Trimethyl-3-[*N*-[3-[2,2,2-trifluoro-*N*-[2-(3-methylbenzamido)ethyl] acetamido] phenyl] sulfamoyl] azulene-1-carboxamide (22).** Compound **14** (0.32 g, 1.0 mmol) and **20** (0.18 g, 0.50 mmol) gave a brown solid, which after flash chromatography (manual gradient of EtOAc/DCM/Toluene 40:59:1 → EtOAc) yielded **22** as a red solid (0.14 g, 44%). ^{1}H NMR (400 MHz, $CDCl_3$) δ 8.91 (d, $J = 10.4$ Hz, 1H), 8.63 (d, $J = 10.0$ Hz, 1H) 8.29 (s, 1H), 7.97 (s, 1H), 7.57 (s, 1H), 7.50 (d, $J = 6.8$ Hz, 1H), 7.42–7.23 (m, 6H), 7.18–7.11 (m, 2H), 6.89–6.88 (m, 2H), 3.73–3.69 (m, 2H), 3.38–3.34 (m, 2H), 3.10–2.97 (m, 6H), 2.66 (s, 3H), 2.35 (s, 3H). HRMS (ESI-QTOF) *m/z*: $[M + H]^+$ Calcd for $C_{32}H_{32}N_4O_5F_3S$ 641.2045; Found 641.2045.

***N,N*-Dimethyl-1-[*N*-[3-[2,2,2-trifluoro-*N*-[2-(3-**

methylbenzamido)ethyl] acetamido] phenyl] sulfamoyl] -3-(2,2,2-trifluoroacetyl)azulene-6-carboxamide (23). Compound **15** (0.15 g, 0.38 mmol) and **20** (0.069 g, 0.19 mmol) gave a red solid, which after two flash chromatographic purifications (manual gradient of DCM → DCM/MeOH 49:1 and DCM/EtOAc 5:5 → 3:7) yielded **23** as a red solid (0.053 g, 38%). ^{1}H NMR (400 MHz, $CDCl_3$) δ 9.95 (d, J = 10.4 Hz, 1H), 9.27 (d, J = 10.4 Hz, 1H), 8.59–5.51 (m, 2H), 7.86 (d, J = 10.0 Hz, 1H), 7.74 (d, J = 10.0 Hz, 1H), 7.46 (s, 1H), 7.42–7.40 (m, 1H), 7.26–7.22 (m, 4H), 7.07 (s, 1H), 6.10–6.99 (m, 1H), 6.76 (t, J = 5.0 Hz, 1H), 3.87–3.85 (m, 2H), 3.54–3.52 (m, 2H), 3.18 (s, 3H), 2.86 (s, 3H), 2.32 (s, 3H). ^{13}C NMR (101 MHz, $CDCl_3$) 176.4 (q, $^2J_{C,F}$ = 35.3 Hz), 170.0, 168.5, 157.9 (q, $^2J_{C,F}$ = 36.3 Hz), 150.7, 145.3, 143.7 (q, $^3J_{C,F}$ = 3.1 Hz), 141.8, 141.4, 139.6, 139.4, 138.7, 138.2, 133.7, 132.7, 132.0, 131.1, 130.7, 128.7, 127.7, 125.2, 125.0, 124.0, 122.7, 122.0, 116.8 (q, $^1J_{C,F}$ = 292.6 Hz), 116.1 (q, $^1J_{C,F}$ = 289.2 Hz), 115.9, 50.9, 39.3, 38.2, 35.6, 21.4. HRMS (ESI-QTOF) m/z: [M + H]$^+$ Calcd for $C_{33}H_{29}N_4O_6F_6S$ 723.1712; Found 723.1714.

***N*^{1},*N*^{1},*N*^{6},*N*^{6}-Tetramethyl-3-[*N*-[3-[2,2,2-trifluoro-*N*-[2-(3-methylbenzamido)ethyl] acetamido] phenyl] sulfamoyl] azulene-1,6-dicarboxamide (24).** Compound **16** (0.097 g, 0.26 mmol) and **20** (0.095 g, 0.26 mmol) gave a blue solid, which after flash chromatography (manual gradient of DCM → DCM/MeOH 24:1) yielded **24** as a purple solid (0.032 g, 18%). ^{1}H NMR (400 MHz, $CDCl_3$) δ 9.10 (d, J = 10.0 Hz, 1H), 8.83 (d, J = 9.2 Hz, 1H), 8.39 (s, 1H), 8.10 (s, 1H), 7.57 (s, 1H), 7.46–7.39 (m, 3H), 7.29–7.27 (m, 2H), 7.24–7.16 (m, 2H), 7.02–6.92 (m, 3H), 3.76–3.73 (m, 2H), 3.40–3.37 (m, 2H), 3.15–2.86 (m, 12H), 2.37 (s, 3H). ^{13}C NMR (101 MHz, $CDCl_3$) δ 170.9, 168.3, 167.1, 157.5 (q, $^2J_{C,F}$ = 36.2 Hz), 148.8, 140.8, 139.6, 139.5, 138.9, 138.7, 138.5, 137.9, 137.4, 134.0, 132.5, 130.3, 128.6, 128.0, 126.8, 126.8, 124.8, 124.1, 122.8, 122.8, 122.2, 121.8, 116.1 (q, $^1J_{C,F}$ = 289.3 Hz), 50.8, 39.4, 37.9, 35.5, 21.5. HRMS (ESI-QTOF) m/z: [M + H]$^+$ Calcd for $C_{34}H_{35}N_5O_6F_3S$ 698.2260; Found 698.2259.

General procedure for the synthesis of compounds 25, 27, 28, 29. An appropriate azulene derivative was suspended in a mixture of MeOH (5.5–22 mL) and H_2O (0.55–2.2 mL). K_2CO_3 (30 equiv) was added and the resulting mixture was stirred at room temperature for 3 h. The reaction mixture was diluted with EtOAc (60 mL) and washed with H_2O (2 × 30 mL) and a saturated aqueous solution of $NaHCO_3$ (30 mL), dried over anhydrous Na_2SO_4, filtered and evaporated to provide a crude product, which was purified by flash chromatography.

3-Methyl-*N*-[2-[[3-[[6-methyl-3-(2,2,2-trifluoroacetyl)azulene]-1-sulfonamido] phenyl] amino] ethyl] benzamide (25). Compound **21** (0.052 g, 0.078 mmol) gave a brown solid, which after flash chromatography (*n*-heptane/(EtOAc:EtOH 3:1) 3:2) yielded **25** as a an orange, amorphous solid (0.017 g, 39%). ^{1}H NMR (400 MHz, DMSO-d_6) δ 10.19 (s, 1H), 9.69 (d, J = 10.4 Hz, 1H), 9.17 (d, J = 10.4 Hz, 1H), 8.41 (t, J = 1.8 Hz, 1H), 8.38–8.37 (m, 1H), 8.18–8.15 (m, 1H), 8.11–8.08 (m, 1H), 7.63–7.59 (m, 2H), 7.34–7.32 (m, 2H), 6.83 (t, J = 8.0 Hz, 1H), 6.34 (t, J = 2.0 Hz, 1H), 6.24–6.22 (m, 2H), 5.73 (t, J = 5.6 Hz, 1H), 3.31–3.27 (m, 2H), 3.03–2.99 (m, 2H), 2.84 (s, 3H), 2.35 (s, 3H). ^{13}C NMR (101 MHz, DMSO-d_6) δ 174.5 (q, $^2J_{C,F}$ = 33.5 Hz), 166.5, 159.2, 149.3, 143.2, 140.4, 140.2 (q, $^3J_{C,F}$ = 4.1 Hz), 139.9, 138.3, 138.2, 137.5, 137.1, 135.9, 134.4, 131.7, 129.5, 128.2, 127.7, 125.0, 124.3, 116.8 (q, $^1J_{C,F}$ = 293.6 Hz), 113.4, 107.9, 107.9, 103.9, 42.3, 38.5, 27.8, 20.9. HRMS (ESI-QTOF) m/z: [M + H]$^+$ Calcd for $C_{29}H_{27}N_3O_4F_3S$ 570.1674; Found 570.1679.

***N*,*N*,6-Trimethyl-3-[*N*-[3-[[2-(3-methylbenzamido)ethyl] amino] phenyl] sulfamoyl] azulene-1-carboxamide (27).** Compound **22** (0.11 g, 0.17 mmol) gave a red solid, which after flash chromatography (manual gradient of DCM → DCM/MeOH 97:3) yielded **27** as a red, amorphous solid (0.049 g, 53%). ^{1}H NMR (400 MHz, DMSO-d_6) δ 9.97 (s, 1H), 9.04 (d, J = 10.0 Hz, 1H), 8.64 (d, J = 10.4 Hz, 1H), 8.44 (s, 1H), 8.00 (s, 1H), 7.67–7.61 (m, 4H), 7.33 (s, 2H), 6.79 (t, J = 7.8 Hz, 1H), 6.36 (s, 1H), 6.23–6.17 (m, 2H), 5.69–5.67 (m, 1H), 3.34 (m, 2H), 3.02–2.91 (m, 8H), 2.72 (s, 3H), 2.35 (s, 3H). ^{13}C NMR (101 MHz, DMSO-d_6) δ 166.5, 166.1, 155.0, 149.2, 138.9, 138.7, 138.4, 137.5, 136.5, 136.4, 135.1, 134.4, 131.7, 130.5, 130.1, 129.3, 128.2, 127.7, 124.3, 121.1, 120.9, 107.4, 107.1, 103.4, 42.4, 38.6, 27.6, 20.9. HRMS (ESI-QTOF) m/z: [M + H]$^+$ Calcd for $C_{30}H_{33}N_4O_4S$ 545.2222; Found 545.2222.

***N*,*N*-Dimethyl-1-[*N*-[3-[[2-(3-methylbenzamido)ethyl] amino] phenyl] sulfamoyl] -3-(2,2,2-trifluoroacetyl)azulene-6-carboxamide (28).** Compound **23** (0.038 g, 0.053 mmol) gave a red solid, which after flash chromatography (manual gradient of DCM → DCM/MeOH 49:1) yielded **28** as a red, amorphous solid (0.025 g, 76%). ^{1}H NMR (400 MHz, $CDCl_3$) δ 9.81 (d, J = 10.4 Hz, 1H), 9.07 (d, J = 10.0 Hz, 1H), 8.65–8.64 (m, 1H), 7.98 (s, 1H), 7.71–7.68 (m, 1H), 7.60–7.57 (m, 1H), 7.51 (s, 1H), 7.46–7.44 (m, 1H), 7.24–7.17 (m, 2H), 7.01–6.98 (m, 1H), 6.85 (t, J = 8.0 Hz, 1H), 6.40–6.38 (m, 1H), 6.27–6.24 (m, 2H), 3.50–3.46 (m, 2H), 3.15 (s, 3H), 3.11–3.08 (m, 2H), 2.84 (s, 3H), 2.29 (s, 3H). ^{13}C NMR (101 MHz, $CDCl_3$) δ 176.4 (q, $^2J_{C,F}$ = 35.1 Hz), 170.1, 168.9, 150.23, 148.9, 145.0, 143.6 (q, $^3J_{C,F}$ = 3.6 Hz), 141.6, 139.6, 138.5, 137.5, 134.0, 132.5, 131.7, 130.7, 130.1, 128.5, 127.9, 125.9, 124.2, 116.8 (q, $^1J_{C,F}$ = 291.9 Hz), 115.7, 111.5, 111.5, 110.6, 106.6, 44.0, 39.4, 39.4, 35.5, 21.4. HRMS (ESI-QTOF) m/z: [M + H]$^+$ Calcd for $C_{31}H_{30}N_4O_5F_3S$ 627.1889; Found 627.1887.

***N*^{1},*N*^{1},*N*^{6},*N*^{6}-Tetramethyl-3-[*N*-[3-[[2-(3-methylbenzamido) ethyl] amino] phenyl] sulfamoyl] azulene-1,6-dicarboxamide (29).** Compound **24** (0.029 g, 0.042 mmol) gave a purple solid, which after flash chromatography (manual gradient of DCM → DCM/MeOH 24:1) yielded **29** as a purple, amorphous solid (0.010 g, 40%). ^{1}H NMR (400 MHz, $CDCl_3$) δ 9.02 (d, J = 10.4 Hz, 1H), 8.81 (d, J = 10.0 Hz, 1H), 8.13 (s, 1H), 7.78–7.74 (m, 1H), 7.64 (s, 1H), 7.59–7.58 (m, 1H), 7.36–7.31 (m, 3H), 7.26–7.23 (m, 2H), 6.83 (t, J = 8.0 Hz, 1H), 6.43 (d, J = 7.6 Hz, 1H), 6.21 (d, J = 8.0 Hz, 1H), 5.89 (s, 1H), 3.28–3.26 (m, 2H), 3.14 (s, 6H), 2.91–2.84 (m, 8H), 2.35 (s, 3H). ^{13}C NMR (101 MHz, $CDCl_3$) δ 171.0, 168.7, 167.3, 148.8, 148.5, 140.8, 139.4, 139.0, 138.4, 138.1, 138.0, 137.6, 134.3, 132.4, 129.9, 128.4, 128.1, 126.4, 124.4, 122.6, 122.6, 111.9, 110.7, 106.3, 44.0, 39.4, 39.3, 35.5, 21.5. HRMS (ESI-QTOF) m/z: [M + H]$^+$ Calcd for $C_{32}H_{36}N_5O_5S$ 602.2437; Found 602.2437.

***N*-[2-[*N*-[3-[(5-Bromo-2-methoxyphenyl)sulfonamido] phenyl] -2,2,2-trifluoroacetamido] ethyl] -3-methylbenzamide (30).** 5-Bromo-2-methoxybenzenesulfonyl chloride (0.78 g, 2.7 mmol) was added to a yellow solution of **20** (1.0 g, 2.7 mmol) and Et_3N (0.76 mL, 5.4 mmol) in anhydrous DCM (11 mL) under argon. The resulting mixture was stirred at room temperature for 48 h. A 1 M aqueous solution of HCl (20 mL) was added and the reaction mixture was stirred at room temperature for an additional 15 min. The mixture was extracted with DCM (30 mL). The organic phase was washed with a 1 M aqueous solution of HCl (20 mL) and brine (20 mL), dried over anhydrous Na_2SO_4, filtered, and evaporated to provide an orange oil. The crude product was purified by flash chromatography (*n*-heptane/(EtOAc:EtOH 3:1) 9:1 → 2:3) to give **30** as a yellowish, amorphous solid (0.96 g, 57%). ^{1}H NMR (300 MHz, $CDCl_3$) δ 7.91 (d, J = 2.4 Hz, 1H), 7.56–7.48 (m, 4H), 7.32–7.20 (m, 4H), 7.09 (s, 1H), 7.00 (d, J = 7.8 Hz, 1H), 6.84 (d, J = 9.0 Hz, 1H), 6.63–6.60 (m, 1H), 3.96–3.93 (m, 5H), 3.65–3.60 (m, 2H), 2.39 (s, 3H). ^{13}C NMR (75 MHz, $CDCl_3$) δ 168.2, 158.2 (q, J = 35.9 Hz), 155.4, 139.6, 138.7, 138.0, 137.9, 134.1, 133.5, 132.6, 130.7, 128.7, 127.8, 127.5, 125.1, 124.0, 122.1, 120.9, 116.2 (q, J = 286.8 Hz), 114.2, 112.9, 56.9, 51.1, 38.3, 21.5. HRMS (ESI-QTOF) m/z: [M + H]$^+$ Calcd for $C_{25}H_{24}N_3O_5BrF_3S$ 614.0572; Found 614.0576.

4′-Methoxy-*N*,*N*-dimethyl-3′-[*N*-[3-[[2-(3-methylbenzamido) ethyl] amino] phenyl] sulfamoyl] [1,1′-biphenyl] -3-carboxamide (1). A mixture of **30** (0.95 g, 1.6 mmol), 3-(*N*,*N*-dimethylaminocarbonyl)benzene boronic acid (0.36 g, 1.9 mmol), Pd(dppf)Cl_2 (0.057 g, 0.078 mmol) and Na_2CO_3 (0.66 g, 6.2 mmol) in 1,4-dioxane (4.8 mL) and H_2O (4.8 mL) was heated at 100 °C for 48 h. The reaction mixture was filtered through a small pad of Celite with EtOAc (150 mL). The organic phase was washed brine (40 mL), dried over anhydrous Na_2SO_4, filtered, and evaporated to provide a brown oil. After two flash chromatographic purifications (*n*-heptane/(EtOAc:EtOH 3:1) 9:1 → EtOAc:

EtOH 3:1 and EtOAc) **1** was obtained as an off-white, amorphous solid (0.48 g, 53%). ^{1}H NMR (400 MHz, DMSO-d_6) δ 9.79 (s, 1H), 8.44 (t, J = 5.6 Hz, 1H), 7.99 (d, J = 2.4 Hz, 1H), 7.89 (dd, J = 8.8, 2.4 Hz, 1H), 7.67–7.64 (m, 2H), 7.62–7.61 (m, 1H), 7.58–7.57 (m, 1H), 7.48 (t, J = 7.8 Hz, 1H), 7.36–7.32 (m, 3H), 7.27 (d, J = 8.8 Hz, 1H), 6.87 (d, J = 8.0 Hz, 1H), 6.42–6.41 (m, 1H), 6.33–6.31 (m, 1H), 6.22 (dd, J = 8.0, 1.6 Hz, 1H), 5.75 (t, J = 5.8 Hz, 1H), 3.94 (s, 3H), 3.36–3.33 (m, 2H), 3.08–3.03 (m, 2H), 2.99 (s, 3H), 2.90 (s, 3H), 2.34 (s, 3H). ^{13}C NMR (101 MHz, DMSO-d_6) δ 169.8, 166.5, 156.2, 149.2, 138.5, 138.4, 137.5, 137.4, 134.4, 133.0, 131.7, 131.2, 129.4, 129.1, 128.1, 128.0, 127.7, 127.3, 127.1, 125.8, 124.6, 124.3, 113.6, 107.3, 107.3, 103.3, 56.4, 42.4, 39.0, 38.6, 34.7, 20.9. HRMS (ESI-QTOF) m/z: $[M + H]^+$ Calcd for $C_{32}H_{35}N_4O_5S$ 587.2328; Found 587.2328.

4.2. Pharmacological analysis

Materials: Human orexin-A was from NeoMPS (Strasbourg, France), *N*-(2-methyl-6-benzoxazolyl)-*N*′-1,5-naphthyridin-4-yl urea (TCS-1102) and *N*-biphenyl-2-yl-1-[[(1-methyl-1*H*-benzimidazol-2-yl)sulfanyl] acetyl]-L-prolinamide (SB334867) from Tocris Bioscience (Bristol, UK), and probenecid from Sigma–Aldrich (St.Louis, MO, USA).

Cell culture and media: CHO-K1 cells expressing human OX_1 and OX_2 receptors cells (CHO-hOX_1 and CHO-hOX_2, respectively),[31–32] and control CHO-K1 cells (not expressing orexin receptors,ctrl CHO cells) were cultured in Ham's F12 medium (Gibco/Life Technologies, Paisley, UK) + supplements on plastic cell culture dishes (56 cm^2 bottom area; Greiner Bio-One GmbH, Frickenhausen, Germany) as previously described.[33–34] Black, clear-bottom half-area Cellstar μClear 96-well cell culture plates (Greiner Bio-One GmbH; Frickenhausen, Germany), coated with polyethyleneimine (25 μg/mL for 1 h at 37 °C; Sigma-Aldrich, St. Louis, MO, USA), were used for Ca^{2+} measurements. Hepes-buffered medium (HBM) consisting of 137 mM NaCl, 5 mM KCl, 1.2 mM $MgCl_2$, 0.44 mM KH_2PO_4, 4.2 mM $NaHCO_3$, 1 mM $CaCl_2$, 10 mM glucose, 20 mM HEPES and 0.1% (w/v) stripped bovine serum albumin (adjusted to pH 7.4 with NaOH) was used as the basic experimental medium.

Ca^{2+} elevation: The compound-induced Ca^{2+} elevations were measured as described before.[35] In brief, CHO-hOX_1, CHO-hOX_2 or control CHO cells were plated on Cellstar plates, 1.5×10^4 cells per well. After 24-hour incubation, the cell culture medium was exchanged to the loading solution consisting of FLIPR Calcium 4 Assay Kit (Molecular Devices, Sunnyvale, CA, USA) dissolved in and diluted with HBM + 1.0 mM probenecid. After subsequent 60 min incubation at 37 °C, intracellular Ca^{2+} levels were measured at 37 °C using a FlexStation 3 fluorescence plate reader (Molecular Devices, excitation at 485 nm, emission at 525 nm). The wells were measured for 150 s with 30 s of baseline before stimulation and measured approximately every 1.3 s. After the measurement, 0.3 nM orexin-A was added to the wells and the plate was re-measured as described above.

Data analysis: Data were visualized using Graph Pad Prism 8 and analysed using Microsoft Excel software. Concentration–response curves were fit using three-parameter nonlinear regression equation. The data points represent the mean ± s.e.m. of 3–5 individual experiments (biological replicates) performed typically in triplicates (technical replicates) unless otherwise stated. All presented Ca^{2+} responses were separately normalized to the control maximum orexin-A or ATP responses for each independent experiment before averaging. The background response (vehicle addition) was subtracted from all data values (both in the single-concentration screen and concentration–response curves) prior to the analysis. Crude estimates of the K_i values were calculated from the inhibition-% values by first estimating the IC_{50}-values and then converting these to K_i utilizing the Cheng–Prusoff equation with cooperativity coefficients. The rational of this follows the Equation (1), which also lies behind the Cheng–Prusoff equation.

$$(100 - \%inhibition)response_{noinhibitor} = \frac{[orexin - A]^n \times (100 - \%inhibition)}{[orexin - A]^n + EC_{50}{}^n} = response_{withinhibitor} = \frac{[orexin - A]^n \times 100}{[orexin - A]^n + EC_{50}{}^n\left(1 + \frac{[I]}{K_i}\right)} \quad (1)$$

4.3. Computational studies

Homology modeling: Our goal was to build a model of OX_1 in an active, agonist-bound, conformation suitable for a subsequent docking study with a small molecule agonist. Thus, we used the active-state cryo-EM structure of OX_2 (PDB ID: 7L1V) as a template. The binding sites of OX_1 and OX_2 are nearly identical as there are only 2–4 conservative differences among the binding site residues, depending on how the site is framed ($S/T^{2.61}$, $S/T^{23.49}$, $A/T^{3.33}$, $S/T^{45.48}$). Prior to building the models, the ligand and residues within 5 Å of the ligand in the OX_2 structure were refined using Prime minimization[36–37] (Schrödinger Release 2020–4). Based on this minimized OX_2 structure, ten models of OX_1 were built consisting of residues $Trp47^{1.33}$-$Trp243^{5.66}$ and $Glu286^{6.23}$-$Ala372^{8.57}$ using MODELLER 10.1[38] with default settings. The N- and C-termini and the ICL3 were not modeled in the cryo-EM structure 7L1V, so they were not included in our models. The model used for the docking study was selected based on the similarity of the binding site residue conformers between the template and the model to facilitate the docking.

Molecular docking of 27: The homology model selected for docking was first preprocessed by Protein Preparation Wizard of Schrödinger Maestro (Schrödinger Release 2020–4) with default parameters, and the hydrogen bond assignments were optimized. Control agonist **31** was docked to the refined OX_2 cryo-EM structure and **27** to the OX_1 homology model using Glide SP[39–41] with default settings and a grid defined by the location of the agonist **31** in the OX_2 complex. The docking poses were analyzed visually in Schrödinger Maestro, and further visualization and figure preparation was carried out with PyMOL 2.3.3 and Gimp 2.10.14. **27** docking poses and homology models are provided as supplementar y files.

Declaration of Competing Interest

The authors declare that they have no known competing financial interests or personal relationships that could have appeared to influence the work reported in this paper.

Data availability

Data will be made available on request.

Acknowledgements

T.O.L. acknowledges the Doctoral Programme in Drug Research of the University of Helsinki and the Academy of Finland (grant no. 330800); A.T. acknowledges the Finnish Cultural Foundation and the Orion Research Foundation; and J.P.K. acknowledges the Magnus Ehrnrooth Foundation, the Liv & Hälsa Foundation and Finska läkaresällskapet for financial support. Marja Peltola, Santeri Suokas and MaijuK. Rinne are acknowledged for assistance with the experiments. We would like to thank Nina Sipari from Viikki Metabolomics Unit (Helsinki Institute of Life Science, University of Helsinki; Biocenter Finland) for her expertise with the LC-MS analyses. CSC – IT Center for Science is thanked for the computational resources.

Appendix A. Supplementary data

Supplementary data to this article can be found online at https://doi.org/10.1016/j.bmc.2023.117325.

References

1 Sakurai T, Amemiya A, Ishii M, et al. Orexins and Orexin Receptors: A Family of Hypothalamic Neuropeptides and G Protein-Coupled Receptors That Regulate Feeding Behavior. *Cell*. 1998;92:573–585. https://doi.org/10.1016/S0092-8674(00)80949-6.

2 de Lecea L, Kilduff TS, Peyron C, et al. The Hypocretins: Hypothalamus-Specific Peptides with Neuroexcitatory Activity. *Proc. Natl. Acad. Sci.* 1998;95:322–327.

3 Kukkonen JP. Physiology of the Orexinergic/Hypocretinergic System: A Revisit in 2012. *Am. J. Physiol. - Cell Physiol.* 2013;301:2–32. https://doi.org/10.1152/ajpcell.00227.2012.

4 Sakurai T. The Role of Orexin in Motivated Behaviours. *Nat. Rev. Neurosci.* 2014;15:719–731. https://doi.org/10.1038/nrn3837.

5 Li, S.-B.; Giardino, W. J.; de Lecea, L. Hypocretins and Arousal. In *Behavioral Neuroscience of Orexin/Hypocretin*; Lawrence, A. J., de Lecea, L., Eds.; Springer International Publishing: Cham, 2017; pp 93–104. https://doi.org/10.1007/7854_2016_58.

6 Schöne C, Burdakov D. Orexin/Hypocretin and Organizing Principles for a Diversity of Wake-Promoting Neurons in the Brain. *Curr. Top. Behav. Neurosci.* 2017;33:51–74. https://doi.org/10.1007/7854_2016_45.

7 James MH, Mahler SV, Moorman DE, Aston-Jones G. A Decade of Orexin/Hypocretin and Addiction: Where Are We Now? *Curr. Top. Behav. Neurosci.* 2017;33:247–281. https://doi.org/10.1007/7854_2016_57.

8 Roecker AJ, Cox CD, Coleman PJ. Orexin Receptor Antagonists: New Therapeutic Agents for the Treatment of Insomnia. *J. Med. Chem.* 2016;59:504–530. https://doi.org/10.1021/acs.jmedchem.5b00832.

9 Sun, Y.; Tisdale, R. K.; Kilduff, T. S. Hypocretin/Orexin Receptor Pharmacology and Sleep Phases. In *Frontiers of Neurology and Neuroscience*; 2021; pp 22–37. https://doi.org/10.1159/000514963.

10 Irukayama-Tomobe Y, Ogawa Y, Tominaga H, et al. Nonpeptide Orexin Type-2 Receptor Agonist Ameliorates Narcolepsy-Cataplexy Symptoms in Mouse Models. *Proc. Natl. Acad. Sci. USA*. 2017;114:5731–5736. https://doi.org/10.1073/pnas.1700499114.

11 Rouet-Benzineb P, Rouyer-Fessard C, Jarry A, et al. Orexins Acting at Native OX1 Receptor in Colon Cancer and Neuroblastoma Cells or at Recombinant OX1 Receptor Suppress Cell Growth by Inducing Apoptosis. *J. Biol. Chem.* 2004;279:45875–45886. https://doi.org/10.1074/jbc.M404136200.

12 Ammoun S, Lindholm D, Wootz H, Åkerman KEO, Kukkonen JP. G-Protein-Coupled OX1 Orexin/Hcrtr-1 Hypocretin Receptors Induce Caspase-Dependent and -Independent Cell Death through P38 Mitogen-/Stress-Activated Protein Kinase. *J. Biol. Chem.* 2006;281:834–842. https://doi.org/10.1074/jbc.M508603200.

13 Voisin, T.; Firar, A. El; Rouyer-Fessard, C.; Gratio, V.; Laburthe, M. A Hallmark of Immunoreceptor, the Tyrosine-Based Inhibitory Motif ITIM, Is Present in the G Protein-Coupled Receptor OX1R for Orexins and Drives Apoptosis: A Novel Mechanism. *FASEB J.* **2008**, *22* (6), 1993–2002. https://doi.org/10.1096/fj.07-098723.

14 El Firar A, Voisin T, Rouyer-Fessard C, Ostuni MA, Couvineau A, Laburthe M. Discovery of a Functional Immunoreceptor Tyrosine- Based Switch Motif in a 7-Transmembrane-Spanning Receptor: Role in the Orexin Receptor OX1R-Driven Apoptosis. *FASEB J.* 2009;23:4069–4080. https://doi.org/10.1096/fj.09-131367.

15 Voisin T, El Firar A, Fasseu M, et al. Aberrant Expression of OX1 Receptors for Orexins in Colon Cancers and Liver Metastases: An Openable Gate to Apoptosis. *Cancer Res.* 2011;71, 3341 LP – 3351.

16 Nagahara T, Saitoh T, Kutsumura N, et al. Design and Synthesis of Non-Peptide, Selective Orexin Receptor 2 Agonists. *J. Med. Chem.* 2015;58:7931–7937. https://doi.org/10.1021/acs.jmedchem.5b00988.

17 Yukitake H, Fujimoto T, Ishikawa T, et al. TAK-925, an Orexin 2 Receptor-Selective Agonist, Shows Robust Wake-Promoting Effects in Mice. *Pharmacol. Biochem. Behav.* 2019;187, 172794. https://doi.org/10.1016/j.pbb.2019.172794.

18 Sabnis RW. Novel 5-Alkyl Pyrrolidine Orexin Receptor Agonists for Treating Sleep Disorders. *ACS Med. Chem. Lett.* 2020;11:2085–2086. https://doi.org/10.1021/acsmedchemlett.0c00501.

19 Zhang D, Perrey DA, Decker AM, et al. Discovery of Arylsulfonamides as Dual Orexin Receptor Agonists. *J. Med. Chem.* 2021;64:8806–8825. https://doi.org/10.1021/acs.jmedchem.1c00841.

20 Hino T, Saitoh T, Nagumo Y, et al. Design and Synthesis of Novel Orexin 2 Receptor Agonists Based on Naphthalene Skeleton. *Bioorg. Med. Chem. Lett.* 2022;59, 128530. https://doi.org/10.1016/j.bmcl.2022.128530.

21 Iio K, Saitoh T, Ohshita R, et al. Discovery of Orexin 2 Receptor Selective and Dual Orexin Receptor Agonists Based on the Tetralin Structure: Switching of Receptor Selectivity by Chirality on the Tetralin Ring. *Bioorg. Med. Chem. Lett.* 2022;60, 128555. https://doi.org/10.1016/j.bmcl.2022.128555.

22 Rinne MK, Leino TO, Turku A, et al. Pharmacological Characterization of the Orexin/Hypocretin Receptor Agonist Nag 26. *Eur. J. Pharmacol.* 2018;837:137–144. https://doi.org/10.1016/j.ejphar.2018.09.003.

23 Iio K, Hashimoto K, Nagumo Y, et al. Design and Synthesis of Orexin 1 Receptor-Selective Agonists. *J. Med. Chem.*. 2023 https://doi.org/10.1021/acs.jmedchem.2c01773.

24 Leino, T. O.; Sieger, P.; Yli-Kauhaluoma, J.; Wallén, E. A. A.; Kley, J. T. The Azulene Scaffold from a Medicinal Chemist's Perspective: Physicochemical and in Vitro Parameters Relevant for Drug Discovery. *Eur. J. Med. Chem.* **2022**. https://doi.org/10.1016/j.ejmech.2022.114374.

25 Leino TO, Turku A, Yli-Kauhaluoma J, Kukkonen JP, Xhaard H, Wallén EAA. Azulene-Based Compounds for Targeting Orexin Receptors. *Eur. J. Med. Chem.* 2018;108:88–100.

26 Turku A, Leino TO, Karhu L, et al. Structure-Activity Relationships of 1-Benzoylazulenes at the OX1 and OX2 Orexin Receptors. *ChemMedChem*. 2019;14:965–981. https://doi.org/10.1002/cmdc.201900074.

27 Leino TO, Baumann M, Yli-Kauhaluoma J, Baxendale IR, Wallén EAA. Synthesis of 1,3,6-Trisubstituted Azulenes. *J. Org. Chem.* 2015;80:11513–11520. https://doi.org/10.1021/acs.joc.5b02271.

28 Hong C, Byrne NJ, Zamlynny B, et al. Structures of Active-State Orexin Receptor 2 Rationalize Peptide and Small-Molecule Agonist Recognition and Receptor Activation. *Nat. Commun.* 2021;12:815. https://doi.org/10.1038/s41467-021-21087-6.

29 Isberg V, Graaf C, Bortolato A, et al. Aligning Topology Maps While Minding the Gaps. *Trends Pharmacol. Sci.*. 2015:36 https://doi.org/10.1016/j.tips.2014.11.001.

30 Ballesteros JA, Weinstein H. Integrated Methods for the Construction of Three-Dimensional Models and Computational Probing of Structure-Function Relations in G Protein-Coupled Receptors. *Methods Neurosci.* 1995;25:366–428.

31 Lund P-E, Shariatmadari R, Uustare A, et al. The Orexin OX1 Receptor Activates a Novel Ca^{2+} Influx Pathway Necessary for Coupling to Phospholipase C. *J. Biol. Chem.* 2000;275:30806–30812. https://doi.org/10.1074/jbc.M002603200.

32 Putula J, Turunen PM, Jäntti MH, Ekholm ME, Kukkonen JP. Agonist Ligand Discrimination by the Two Orexin Receptors Depends on the Expression System. *Neurosci. Lett.* 2011;494:57–60. https://doi.org/10.1016/j.neulet.2011.02.055.

33 Jäntti MH, Putula J, Somerharju P, Frohman M, Kukkonen JP. OX1 Orexin/Hypocretin Receptor Activation of Phospholipase D. *Br. J. Pharmacol.* 2012;165:1109–1123. https://doi.org/10.1111/j.1476-5381.2011.01565.x.

34 Holmqvist T, Åkerman KEO, Kukkonen JP. Orexin Signaling in Recombinant Neuron-like Cells. *FEBS Lett.* 2002;526:11–14. https://doi.org/10.1016/S0014-5793(02)03101-0.

35 Turku, A.; Rinne, M. K.; Boije af Gennäs, G.; Xhaard, H.; Lindholm, D.; Kukkonen, J. P. Orexin Receptor Agonist Yan 7874 Is a Weak Agonist of Orexin/Hypocretin Receptors and Shows Orexin Receptor-Independent Cytotoxicity. *PLoS One* **2017**, *12* (6), e0178526.

36 Jacobson MP, Pincus DL, Rapp CS, et al. A Hierarchical Approach to All-Atom Protein Loop Prediction. *Proteins Struct. Funct. Bioinforma.* 2004;55:351–367. https://doi.org/10.1002/prot.10613.

37 Jacobson MP, Friesner RA, Xiang Z, Honig B. On the Role of the Crystal Environment in Determining Protein Side-Chain Conformations. *J. Mol. Biol.* 2002;320:597–608. https://doi.org/10.1016/S0022-2836(02)00470-9.

38 Šali A, Blundell TL. Comparative Protein Modelling by Satisfaction of Spatial Restraints. *Journal of Molecular Biology*. 1993;234:779–815. https://doi.org/10.1006/jmbi.1993.1626.

39 Friesner RA, Banks JL, Murphy RB, et al. Glide: A New Approach for Rapid, Accurate Docking and Scoring. 1. Method and Assessment of Docking Accuracy. *J. Med. Chem.* 2004;47:1739–1749. https://doi.org/10.1021/jm0306430.

40 Halgren TA, Murphy RB, Friesner RA, et al. Glide: A New Approach for Rapid, Accurate Docking and Scoring. 2. Enrichment Factors in Database Screening. *J. Med. Chem.* 2004;47:1750–1759. https://doi.org/10.1021/jm030644s.

41 Friesner RA, Murphy RB, Repasky MP, et al. Extra Precision Glide: Docking and Scoring Incorporating a Model of Hydrophobic Enclosure for Protein−Ligand Complexes. *J. Med. Chem.* 2006;49:6177–6196. https://doi.org/10.1021/jm051256o.